

# A Combined Theoretical/Experimental Approach for Reducing Ringing Artifacts in Low Dynamic Testing with Servo-hydraulic Load Frames

X. Yang · L.G. Hector Jr. · J. Wang

Received: 26 April 2013 / Accepted: 5 January 2014 / Published online: 28 January 2014  
© Society for Experimental Mechanics 2014

**Abstract** One of the most challenging tasks facing computer-aided engineering (CAE) analysis is the acquisition of accurate tensile test data that spans quasi-static to low dynamic ( $10^{-5}/s \leq \dot{\epsilon} \leq 5 \times 10^2/s$ ) strain rates ( $\dot{\epsilon}$ ). Critical to the accuracy of data acquired over the low dynamic range is the reduction of ringing artifacts in flow data. Ringing artifacts, which are a consequence of the inertial response of the load frame, are spurious oscillations that can obscure the desired material response (i.e. load vs. time or load vs. displacement) from which flow data are derived. These oscillations tend to grow with increasing strain rate and peak at the high end of the low dynamic range on servo-hydraulic tensile test frames. Common practices for addressing ringing are data filtering, which is often problematic since filtering introduces distortion in smoothed material data, or trial-and-error design of test specimen geometries. This renders techniques for reducing ringing based upon the mechanics of the load frame and optimization of tensile specimen geometry quite attractive. In the present paper, relationships between load, stress wave propagation, and specimen geometries are addressed, to both quantify ringing and to develop specimen designs that will reduce ringing. A combined theoretical/experimental approach for tensile specimen design was developed for reducing ringing in flow data over the low dynamic range of strain rates ( $10^{-5}/s \leq \dot{\epsilon} \leq 5 \times 10^2/s$ ). The single

camera digital image correlation (DIC) method was used to measure the displacement fields and strain rates with specimens resulting from the combined theoretical/experimental approach. While the approach was developed on a specific commercial load frame with a TRIP steel subject to a two-step quenching and partitioning heat treatment (Q&P980), it is readily adaptable to other servo-hydraulic load frames and metallic alloys. The developed approach results in a 90 % reduction in ringing artifact (with no filtering) in a tensile flow curve for Q&P980 at  $\dot{\epsilon} = 5 \times 10^2/s$ . Results from split Hopkinson bar tests of Q&P980 were performed at  $\dot{\epsilon} = 500/s$  and compare favorably with the test data generated by the developed testing approach. Since the Q&P980 steel represents a new generation of advanced high strength steels, we also evaluated its strain rate sensitivity over the low dynamic range.

**Keywords** Low dynamic strain rate · Tensile specimen design · Load cell ringing · Load measurement · Strain rate sensitivity

## Introduction

Global transportation industries are under increasing pressure from government agencies and consumer advocate groups to produce safer and more durable vehicles while improving fuel economy and emission standards. Over the years, new and existing material and joining technologies have been introduced to achieve the goal of lightweighting. In order to comply with various safety regulations, vehicle design engineers in the automotive industry (for example) must have sufficient information and knowledge about material strength and other mechanical properties when new materials are introduced to a specific vehicle design. Since computer-aided engineering (CAE) simulations are being increasingly used for structural analyses under impact conditions, it is necessary

---

X. Yang (✉) · J. Wang  
China Science Lab, General Motors, Shanghai 200120, People's Republic of China  
e-mail: xin.x.yang@gm.com

X. Yang  
e-mail: xin\_x\_yang@163.com

J. Wang  
e-mail: jeff.wang@gm.com

L.G. Hector Jr.  
GM Research & Development, 30500 Mound Road, Warren, MI 48090-9055, USA  
e-mail: louis.hector@gm.com



to characterize the deformation and fracture of materials with accurate mechanical properties.

Uniaxial tensile test data provides material flow behavior, which can be used to generate material parameters for conducting finite element (FE) simulations of vehicle crash events. Tensile testing typically involves elongating a dog-bone specimen (cut from a metal sheet 1–2 mm in thickness) to fracture at a specified nominal strain rate ( $\dot{\epsilon}$ ) in an instrumented load frame. The range of  $\dot{\epsilon}$  values associated with material flow behavior for vehicle crash simulations span quasi-static to low dynamic strain rates,  $10^{-5}/s \leq \dot{\epsilon} \leq 5 \times 10^2/s$ , although rates that exceed the  $5 \times 10^2/s$  upper limit have been reported [1–3]. This testing range addresses the fact that deformation rates of steel components (for example) in a crash event can reach up to several hundreds of  $\dot{\epsilon}$  [4]. In addition, the  $\dot{\epsilon}$  range accounts for effects of  $\dot{\epsilon}$  sensitivity (or the change in flow stress as a function of strain rate) observed in many automotive alloys [5]. Examples of rate sensitive materials of relevance to the automotive industry are dual phase, quenched boron (or press hardened), TRIP, and interstitial free (IF) steels [5–9], and various aluminum alloys [10, 11].

Servo-hydraulic testing machines are usually employed to generate the data for material flow behavior in the so-called low dynamic (or intermediate) deformation range ( $10/s \leq \dot{\epsilon} \leq 5 \times 10^2/s$ ) [3, 4]. The low dynamic testing range is especially challenging since it involves rates that are faster than the quasi-static equilibrium of a conventional quasi-static tensile test, but slower than a split-Hopkinson bar test ( $5 \times 10^2/s \leq \dot{\epsilon} \leq 10^4/s$ ), which is a common dynamic test for material properties [12, 13]. The deformation of the tensile specimen is not at equilibrium for the duration of the test and the material response is affected by stress waves that propagate through the load train (which defines the load path from the tensile specimen to the load cell) [3]. Stress waves result from the sudden engagement of the upper portion of the load train that cause oscillations at the natural frequency of the test system known as “ringing”. Ringing appears as a spurious oscillatory signal superimposed onto the “true” material response (e.g. load vs. time or load vs. displacement) as the test specimen is not in equilibrium for the duration of the test. This can obscure the desired material response leading to inaccurate flow data [14–21]. The ringing frequencies of typical load cells fall in the 2,400 Hz to 3,600 Hz range [1].

Most test frame manufacturers provide the means for reducing ringing through judicious attention to load train designs and various filtering techniques that result in “smoothed” material data. A common theoretical approach aimed at modeling sources of ringing in load frames for dynamic tests is modal analysis of the load train (e.g. load cell, gripping mechanism components, test specimen geometry) which reveals sources of undesirable signals in the load

train [11, 22, 23]. However, uncertainties often remain regarding the accuracy of smoothed material data since filtering is in and of itself intentional distortion [24].

At the present time, existing recommendations for dynamic testing as well as related articles in the literature have uniformly recognized the importance of tensile specimen design as a means for reducing ringing [22, 25]. Specimen designs in low dynamic tests result from either extensive trial-and-error or by following a set of “guidelines” that have little quantitative connection to the dynamics of the testing load frame [15]. This renders theoretical techniques that suggest a dog-bone tensile specimen geometry for reducing ringing in servo-hydraulic test frames all the more desirable. Unfortunately, theoretical approaches that aim to optimize tensile specimen design to minimize (or even eliminate) system ringing in dynamic testing could not be located in the extant literature. Instead, focus has mostly been on tensile specimen designs that achieve a uniaxial stress state during dynamic testing [9], or on reduction of ringing through data filtering [23].

In this paper, we develop a combined theoretical/experimental approach based upon the dynamics of a commercial servo-hydraulic load frame, to optimize the specimen geometry for reducing ringing artifacts in tensile flow curves acquired over the low dynamic strain rate range of  $10/s \leq \dot{\epsilon} \leq 5 \times 10^2/s$ . Tensile tests were conducted with a ZWICK dynamic load frame. Relationships between load, stress wave propagation, and specimen geometries are addressed, to both quantify ringing and then used to develop tensile specimen designs that will reduce ringing. Tensile specimens consisting of a TRIP steel subject to quenching and partitioning (Q&P), a third generation advanced high strength steel, are tested over the low dynamic range of strain rates, and the extent to which ringing is reduced in the flow curves is examined. The flow data from split Hopkinson bar tests of Q&P980 were acquired at  $\dot{\epsilon} = 500/s$ , and show very favorable agreement with the test data generated by the combined theoretical/experimental approach to reduce ringing detailed herein.

### Modal Analysis of Load Train

As discussed by Xiao et al. [14], stress waves can pass through the load train (i.e. load path from the test specimen to the load cell) under the low dynamic range of strain rates, and cause ringing of a servo-hydraulic test system. Ringing can obscure the desired material response leading to inaccurate flow data. Modal analyses of the load frame have been developed to evaluate the load train [11, 22, 23] in an attempt to reduce ringing over the low dynamic range. The most common approach is to use a single degree-of-freedom spring-mass-damper (SMD) model to represent the load train [22, 23]. This

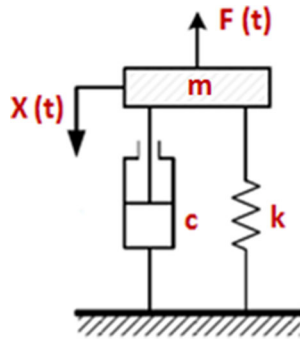


**Fig. 1** Single degree-of-freedom spring-mass-damper (SMD) model. The input signal to the SMD model is  $F(t)$  which corresponds to the material response of the specimen in the low dynamic tensile test. The output of the SMD model is  $X(t)$ ; this represents the elastic deformation of the SMD model, which corresponds to the measurement of load cell.  $m$  is the mass of the grip connecting the test specimen and the load cell;  $k$  and  $c$  are the stiffness and viscous damping of the load train, respectively

approach identifies the dominant factors for the reduction of ringing under the low dynamic range, which we briefly review in the following developments. Figure 1 illustrates a typical SMD model, including mass ( $m$ ), stiffness ( $k$ ), and viscous damping ( $c$ ). The input signal to the SMD model is  $F(t)$ , which corresponds to the resistance of the tensile specimen to the load frame force. The output of the SMD model is  $X(t)$ , which represents the spring deformation in the SMD model. Based on a Hooke's law-type relationship,  $X(t)$  can be converted to force data from a load cell. The oscillatory profile of  $X(t)$  is indicative of ringing in the load cell measurement during the test. The equation of motion for the SMD model is given by,

$$m \frac{d^2X(t)}{dt^2} + c \frac{dX(t)}{dt} + kX(t) = F(t) \quad (1)$$

The initial conditions of equation (1) are,  $X(0) = 0$ , and  $\dot{X}(0) = 0$ . Laplace transformation of equation (1) gives

$$ms^2X(s) + csX(s) + kX(s) = F(s) \quad (2)$$

where  $X(s)$  and  $F(s)$ , respectively, represent the Laplace transforms of  $X(t)$  and  $F(t)$ . Solving equation (2) for the transform function (which describes the relationship between the input and output of the SMD model) gives

$$H(s) = \frac{X(s)}{F(s)} = \frac{1}{ms^2 + cs + k} = \frac{1/m}{s^2 + \frac{c}{m}s + \frac{k}{m}} \quad (3)$$

Equation (3) can be simplified by applying the following definitions:

- (1)  $\omega_n^2 = \frac{k}{m}$ , where  $\omega_n$  is the natural circular frequency of an undamped oscillation ( $c = 0$ ).

- (2)  $\zeta = \frac{c}{2\sqrt{km}}$ , where  $\zeta$  represents the damping ratio.  $\zeta$  is a dimensionless factor describing how an oscillation can decay. A larger value of  $\zeta$  denotes a faster rate of decay of an oscillation.

Using the above substitutions, the transform function can be rewritten as,

$$H(s) = \frac{1/k}{\left(\frac{s}{\omega_n}\right)^2 + 2\zeta \frac{s}{\omega_n} + 1} \quad (4)$$

Assuming both  $F(t)$  and  $X(t)$  are sinusoidal functions with circular frequency of  $\omega$ , the frequency response of the transform function can be derived from the following:

$$|H(j\omega)| = \frac{1/k}{\sqrt{\left(1 - \left(\frac{\omega}{\omega_n}\right)^2\right)^2 + 4\zeta^2 \left(\frac{\omega}{\omega_n}\right)^2}} \quad (5)$$

$$\phi(\omega) = \arctan\left(\frac{2\zeta}{\omega/\omega_n - \omega_n/\omega}\right) \quad (6)$$

where  $|H(j\omega)|$  and  $\phi(\omega)$  represent the amplitude and the phase angle of the transform function, respectively. The frequency response of the transform function can help to identify unwanted frequencies in  $F(t)$  (input to the load train), which can cause ringing.

To understand how quickly the ringing of the load train can decay, a unit step signal ( $F(t) = 1$  N) was input to the SMD model. Vibrational responses of the SMD model in equation (1) at different values of  $\zeta$  were calculated and are displayed (in the time domain) in Fig. 2. When  $X(t) = 1$  mm, the load cell produces a measurement that can 100 % represent the load from the test specimen. For  $\zeta \geq 0.8$ , no oscillations appear; however, the system needs a relatively long time to converge to  $X(t) = 1$  mm. In this case, the load cell is not appropriate for testing under conditions where low dynamic strain rates are prevalent, and can only be applied for tensile tests at quasi-static strain rates. For values of  $\zeta$  below 0.6, Fig. 2 shows that the peak oscillation amplitude gradually increases, and then decays with time, and hence a longer time is required for the input excitation to decay. The ideal convergence rate for no ringing during the low dynamic range occurs when  $0.6 \leq \zeta \leq 0.8$ .

As pointed out by Irvine et al. [26],  $0.05 \leq \zeta \leq 0.2$  can be usually achieved in a commercial servo-hydraulic tester that uses nearly undamped connections (e.g. bolts) to connect a test specimen and grippers or load cell and grippers. In order

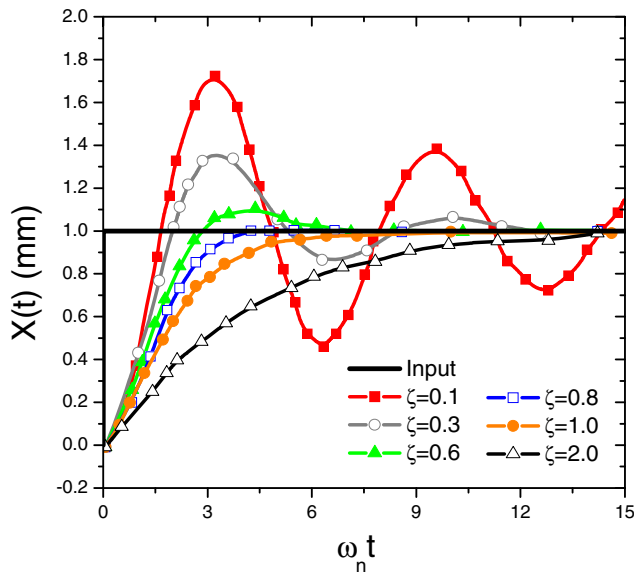


**Fig. 2** Load cell response  $X(t)$  due to a unit impulse,  $F(t)=1$  N for different values of the damping ratio,  $\zeta$ . Note that  $\omega_n$  is the natural circular frequency of the SMD model in equation (1).  $X(t)$  is the output of the SMD model, which corresponds to the measurement of the load cell in a dynamic testing system. The faster  $X(t)$  decays to zero, the less likely ringing artifacts will occur in the tensile flow curves

to understand how  $\omega$  (which is the frequency of  $F(t)$ ) can affect ringing, especially under low damping conditions ( $\zeta < 0.2$ ),  $|H(j\omega)|k$  vs.  $\omega$  curves were calculated. A  $|H(j\omega)|k$  vs.  $\omega$  curve with zero oscillations is necessary to produce a load cell measurement with no ringing. Figure 3 presents the results of  $|H(j\omega)|$  under different input frequencies. For  $\zeta < 0.2$ ,  $|H(j\omega)|$

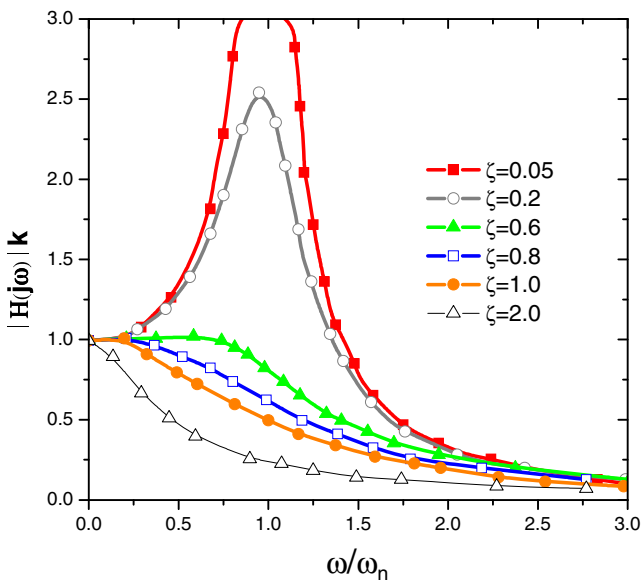


**Fig. 3** Magnitude of transform function ( $H(j\omega)$ ) as a function of input frequency.  $|H(j\omega)|k$  derived from the solution of equation (1) is the magnitude factor, reflecting the input signal frequencies at which the load cell is likely to significantly vibrate. Note that  $\zeta$  represents the damping ratio of the SDS model.  $\omega_n$  is the natural circular frequency of the SMD model.  $\omega$  represents the circular frequency of the input signal to the SMD model

can stay at a constant value for values of  $\omega$  that are substantially smaller than  $\omega_n$ . The curve starts to significantly oscillate as  $\omega/\omega_n > 0.25$  for  $\zeta = 0.05$  and  $\zeta = 0.2$ . Hence, this analysis suggests that the natural frequency of the test system  $\omega_n$ , should be at least four times higher than that of the input signal  $\omega$ , which also corresponds to the frequency of the load-time response of the tensile specimen up to fracture. Additional tests of the steel material (subsequently described in Section 5), which was the test material of choice in this paper, confirmed that the SMD model effectively removed the ringing at the low dynamic range of strain rates for the complex specimen/load cell system.

### Assessment of the Load Train with a Servo-Hydraulic Tester

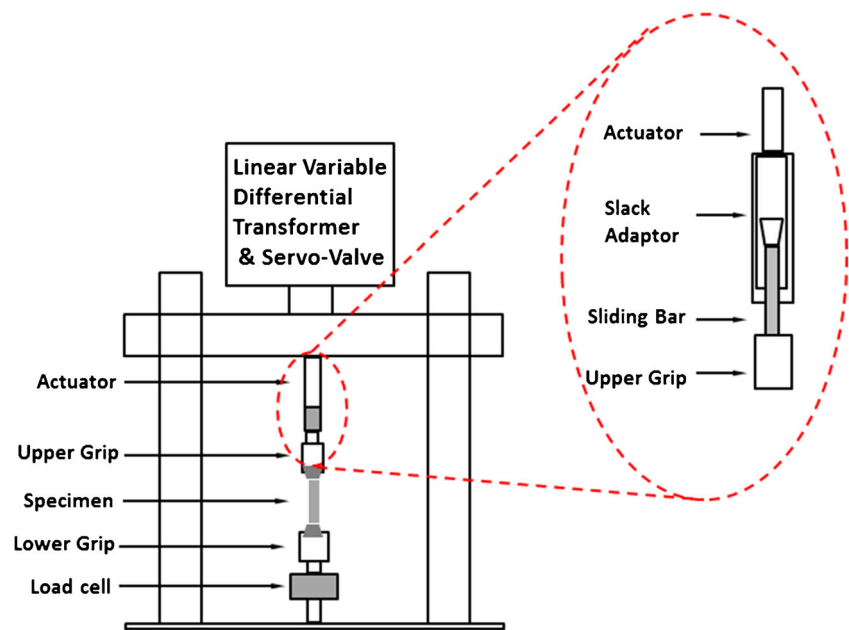
Figure 4 is a schematic diagram of the servo-hydraulic tensile testing machine used in this study. This schematic is based upon the ZWICK HTM5020 load frame. It consists of a load cell, upper and lower grips, a test specimen and a servo-hydraulic loading device. The machine can achieve a maximum testing speed of 20 m/s and has a load capacity of 50 kN. Dynamic load is introduced to the upper grip through a slack adaptor and a sliding bar with a cone-shaped end. When the machine is actuated, the slack adaptor travels freely with the actuator to reach a specified velocity before making contact with the cone-shaped end of the sliding bar that is connected to the upper grip. After that, the test specimen is accelerated, and load is transferred to the lower grip and the load cell. Therefore, the load train of the ZWICK tester consists of the test specimen, the lower grip and the tester load cell. The actuator can travel at a constant velocity during the loading process which imposes a nearly constant loading rate on the specimen. The mass of the lower grip, which is placed between the test specimen and load cell, can have an effect on the ringing of the load cell. This inertial effect can be reduced by decreasing the mass of lower grip [17, 27]. The sudden engagement of the upper portion of the load train generates a high amplitude stress wave in the specimen. This stress wave excites the load train, and causes ringing.

The natural circular frequency of the load train (from test specimen to tester load cell) of the ZWICK tester is,  $\omega_n = 9.92$  kHz. The approach to evaluate the natural circular frequency of the load train for a commercial tester was briefly described in [28]. The critical circular frequency of  $F(t)$  (which is the load signal introduced to the load train),  $\omega_c$ , is evaluated via

$$\omega_c = \omega_n/4 = 2.48 \text{ kHz} \quad (7)$$

Based on the analysis in Section 2, the ringing in the tester load cell measurement during the low dynamic tensile test should be eliminated for  $\omega \leq \omega_c$ . The critical strain rate  $\dot{\epsilon}_c$ , which corresponds to  $\omega_c$  at 2.48 kHz, is equal to 120/s (please

**Fig. 4** Schematic diagram of the high speed testing machine



refer to Appendix 1 which details the conversion of  $\omega$  to  $\dot{\epsilon}$ ). Therefore, the maximum  $\dot{\epsilon}$  at which the ZWICK tester load cell can be used to generate the true material response without ringing artifact is 120/s.

A low dynamic tensile test was performed with the ZWICK load frame using a Q&P980 steel (a TRIP steel subject to a two-step quenching and portioning process – see Appendix 2 for additional details) test specimen. Figure 5 presents the dynamic test results of Q&P980 steel, in which the gauge length and width of the tensile test specimen are, respectively, 25 mm and 6 mm. As shown in Fig. 5a, a reasonably smooth tensile test curve was achieved at  $\dot{\epsilon} = 100/s$  ( $\dot{\epsilon} < \dot{\epsilon}_c$ ). Figure 5b shows that as  $\dot{\epsilon}$  increased to 300/s ( $\dot{\epsilon} > \dot{\epsilon}_c$ ), severe oscillations due to load cell signal ringing appeared (black curve). Note that  $\omega$  is equal to 7.34 kHz at 300/s, which is almost the same as  $\omega_n$  of the load train: this is the cause of the oscillations at  $\omega_n$  of the tester load cell.

A standard practice for minimizing ringing in the low dynamic test range is to apply a filter. The solid red curve in Fig. 5b resulted from low-pass filtering via Fast Fourier Transform (FFT) of the profile from the raw data in the solid black curve. A cut-off frequency of 9.92 kHz (which is equal to  $\omega_n$  of the ZWICK tester) was used. The ringing artifact is reduced, but not completely eliminated by low-pass filtering. Hence, there is still substantial uncertainty about the true material response in the filtered curve of Fig. 5b. This suggests that testing in the low dynamic range of strain rates with the ZWICK tester must be modified to increase  $\omega_n$  of the load train to more efficiently and effectively remove ringing artifacts. We surmise that this

observation is by no means unique to the ZWICK tester and the same approach would be required for other commercial testers.

### Tensile Specimen Design for Reducing Ringing Artifacts

#### Specimen Design

In this section, the load train of the ZWICK servo-hydraulic load frame (shown schematically in Fig. 4) was modified to increase  $\omega_n$  of the load train and to minimize ringing artifacts in the material response. As shown in Fig. 6a, a strain gauge was attached on the fixed end of test specimen (we note that this is a common technique in servo-hydraulic testing). Instead of the load cell on the tester, the strain gauge was applied for load measurement as

$$F = ES\varepsilon \quad (8)$$

where  $E$  is the Young's modulus of test specimen;  $S$  is the cross-sectional area of the fixed end of test specimen ( $S = \text{width of the fixed end} \times \text{specimen thickness}$ );  $\varepsilon$  is the strain data measured by the strain gauge. The strain gauge is a new "load cell", directly attached on the test specimen. Using the strain gauge for load measurement is a routine practice and can also be found in [15–20] for low dynamic testing. In this case, the load train was re-designed to only include the test specimen between the upper grip and lower grip. Since the load is constant through the specimen (the stress equilibrium of the test specimen is subsequently analyzed in Section 4.2),

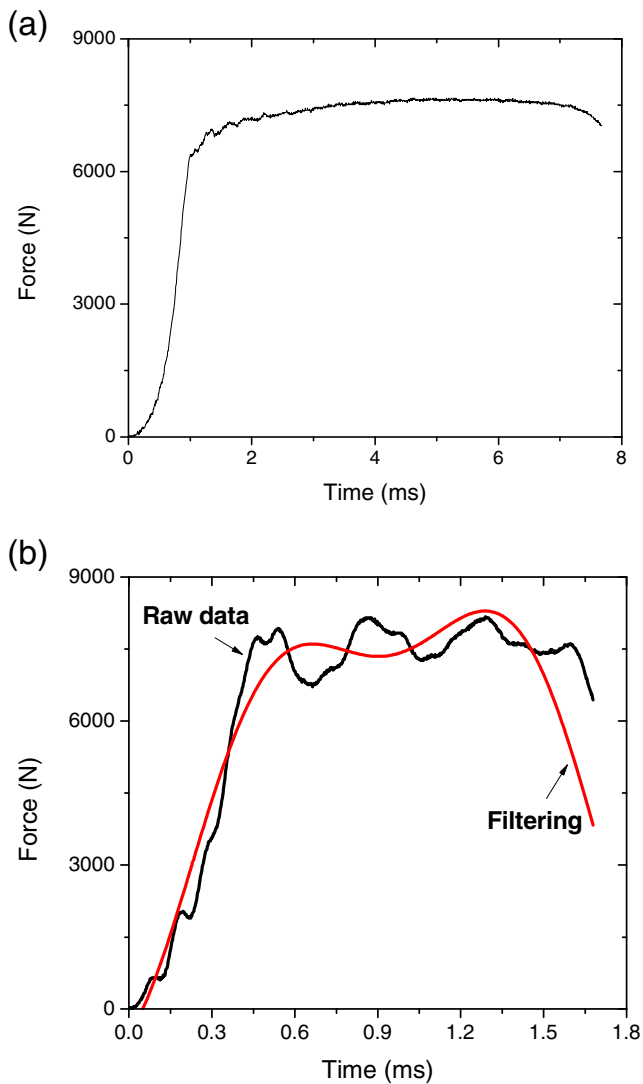


**Fig. 5** Force-time curves from dynamic tensile tests (Q&P980): **a**  $\dot{\epsilon} = 100/s$ , and **b**  $\dot{\epsilon} = 300/s$ . *Black curve*: raw data; *red curve*: filtered data

the flow curve of the test material can be generated by the load data measured from the strain gauges.

Referring to Fig. 6b, we assume the specimen gauge length and width are, respectively,  $L1$  and  $W1$ . The length of the upper (movable) end and the lower (fixed) end of the tensile specimen are, respectively,  $L2$  and  $L3$ . The widths of the upper and lower ends are, respectively,  $W2$  and  $W3$ . The length of the gripping regions at both end is  $L_G$ , and the tensile specimen thickness is  $T$ . The natural circular frequency of the tensile specimen,  $\omega'_n$ , is defined by

$$\omega'_n = \sqrt{K'/M} \quad (9)$$

where  $K'$  and  $M$  represent the effective stiffness and mass of the test specimen, respectively. As depicted in Fig. 6b, the reduced sections of the tensile specimen were not considered. For convenience in the ensuing developments, the tensile specimen

was divided into three regions with rectangular shapes. Hence,  $K'$  is associated with the superposition of three terms

$$1/K' = 1/K_1 + 1/K_2 + 1/K_3 \quad (10)$$

in which

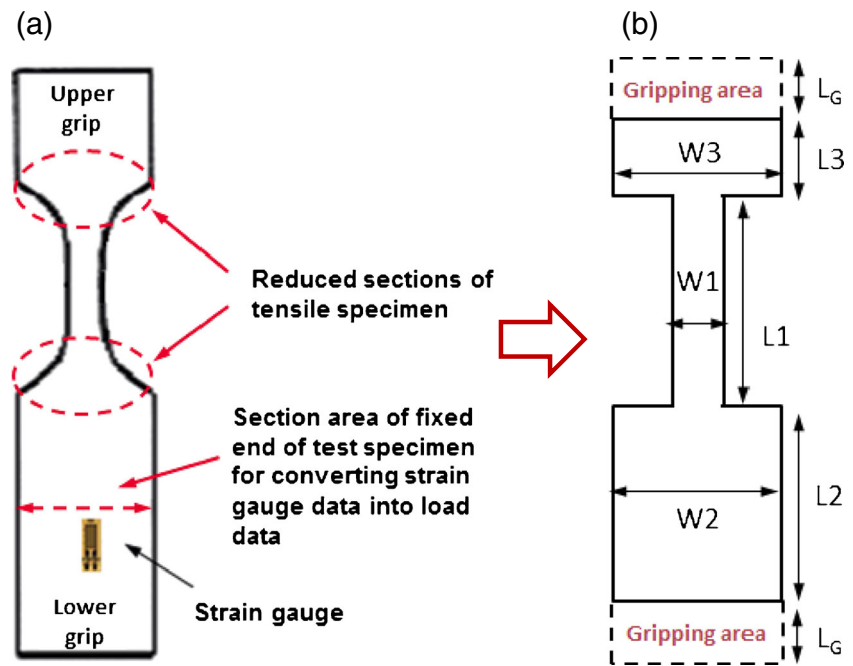
$$K_i = \frac{F}{\Delta L_i} = \frac{E(\Delta L_i/L_i)W_iT}{\Delta L_i} = EW_iT/L_{i(i=1,2,3)} \quad (11)$$

defines the stiffnesses of the tensile specimen gauge region ( $i=1$ ), i.e. the lower ( $i=2$ ) and upper ( $i=3$ ) grip regions. Also,  $\Delta L_i$  is the elongation of each rectangle region;  $E$  is Young's modulus of the tensile specimen, which is assumed to be known before the tests (for Q&P980 steel,  $E = 207$  GPa).

The dimensions of both gripping areas were determined by the grippers of the ZWICK load frame, i.e.,  $W2=W3=25$  mm, and  $L_G=35$  mm. In order to reduce the total length of the tensile test specimen, it was determined that  $L3=10$  mm. Furthermore, to achieve a uniaxial stress state, the width of the gauge section needs to be much smaller than that of the gripping ends [28], e.g.,  $W1=W2/4=6$  mm. In order to determine  $L2$ , a parametric study was performed. As an example, tensile tests of Q&P980 using specimens with different values of  $L2$  (in which  $L1=35$  mm) were conducted at 500/s. The results are shown in Fig. 7. It can be seen that as  $L2$  increases, the ringing artifact is reduced. The ringing converged to an amplitude of 500 N as  $L2 \geq 45$  mm. Therefore,  $L2$  in Fig. 6b was set to 45 mm for Q&P980 steel. In this way,  $L1$  is the only parameter that needs to be optimized based on the condition for no ringing of the load train ( $\omega_n \geq 4\omega$ ). At  $\dot{\epsilon} = 500/s$ ,  $\omega$  is 8.42 kHz (please refer to Appendix 1 which details the conversion of  $\omega$  to  $\dot{\epsilon}$ ). In order to avoid system ringing in the low dynamic range of strain rates ( $10/s \leq \dot{\epsilon} \leq 5 \times 10^2/s$ ), the natural circular frequency of the load train must be  $\omega'_n \geq 4\omega = 33.68$  kHz. We introduced  $W_i$  and  $L_i$  determined above into equations (10) and (11) to calculate  $K'$ , and then used this to solve equation (9) for  $L1$ . It was determined that,  $L1 \leq 25$  mm. The recommended dimensions of test specimen for the low dynamic range of strain rates with the ZWICK load frame are presented in Fig. 8a. Unlike other approaches detailed in the literature [14–21], which use a trial-and-error method to determine the tensile test specimen geometries for reducing the ringing, the present combined experimental/theoretical approach based upon analysis of the load train leads naturally to the optimal test specimen dimensions that minimize ringing.

Figure 9 compares the Q&P980 force-time curves at 500/s for tensile specimens with  $L1=25$  mm (Fig. 9a) and  $L1=35$  mm (Fig. 9b). Note that  $\omega'_n = 34$  kHz for the 25 mm gauge length, but it is  $\omega'_n = 21$  kHz for the 35 mm gauge length based upon equations (9)–(11). As shown in Fig. 9b, when  $L1 > 25$  mm, ringing with an amplitude of 500 N was observed in the force-time

**Fig. 6** Design of specimen dimensions: **a** specimen for dynamic tensile test, and **b** simplified tensile specimen in which the reduced section of the tensile specimen is not considered. The gauge length and width are  $L1$  and  $W1$ , respectively. The lengths of the upper (movable) end and the lower (fixed) end of the tensile test specimen are, respectively,  $L2$  and  $L3$ . The widths of the upper and lower ends are, respectively,  $W2$  and  $W3$ . The length of the gripping area at both ends is  $L_G$



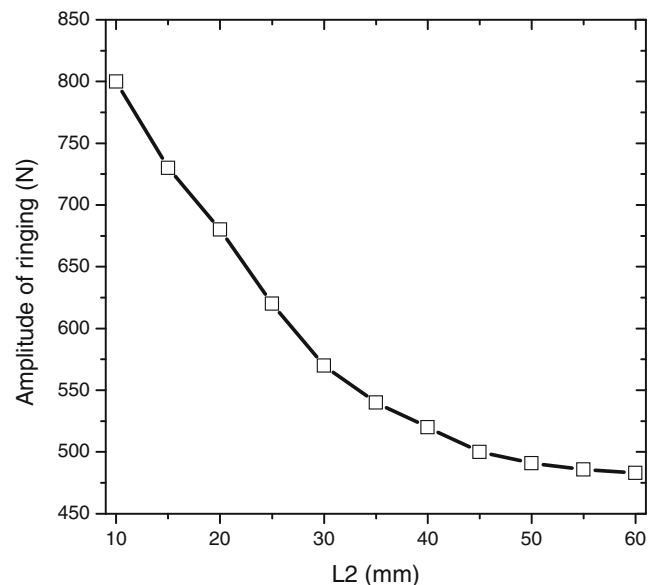
signal. But no ringing was produced with the optimized tensile specimen dimensions of  $L1=25$  mm (as shown in Fig. 9a). Therefore, using the tensile specimen dimensions for Q&P980 suggested from the present approach minimized the ringing artifact over the low dynamic range in the load train by at least 90 %. If in fact a different material is to be tested, the preceding analysis will need to be repeated to determine  $\omega_n \geq 4\omega$ . For example, the gauge length ( $L1$ ) of an aluminum material would be shorter than that of Q&P980, since the Young's modulus of aluminum is lower relative to steel (for aluminum,  $E=70$  GPa). However, the present approach can only be applied to a material with rate-independent Young's modulus (e.g. aluminum, copper, or magnesium), in which the Young's modulus can be determined by a quasi-static tensile test, but is independent of strain rate.

Figure 10 depicts the upper fixture of the ZWICK load frame. The movable fixture is designed to rotate during a tensile test, resulting in a bending moment applied to the test specimen. This bending moment also contributes to ringing, and hence, must be quantified and extracted. To address this, two strain gauges were symmetrically placed on the fixed end of a test specimen as shown in Fig. 8b. The data measured by the two strain gauges were added together to calculate the load on the mid-plane of the specimen. Since no bending was applied on the mid-plane of the specimen, the bending effect can be removed from the load-time signal. As illustrated in Fig. 11, with a single strain gauge, a significant ringing phenomenon produced by the transverse bending moment can be observed from both strain gauge voltages. The average result using two strain gauges is considerably smoother, and thereby, reliable for a dynamic tensile test at low dynamic strain rates. Two strain gauges, to remove the bending effect from load measurement of tensile specimen, are

recommended for dynamic tensile tests. Note that although the present combined theoretical/experimental approach was developed on the ZWICK tester, it can be readily adapted to other load frames with a hydraulic system. However, the approach would not be used for a tensile Hopkinson bar system for testing at strain rates of thousands per second.

#### Stress Equilibrium

There are two major challenges with low dynamic tensile testing. The first is the ringing artifact from the load train,



**Fig. 7** Effect of  $L2$  on the amplitude of the ringing artifact for a Q&P980 tensile specimen at 500/s.  $L2$  represents the length of the lower end (fixed) of the tensile test specimen as shown in Fig. 6b

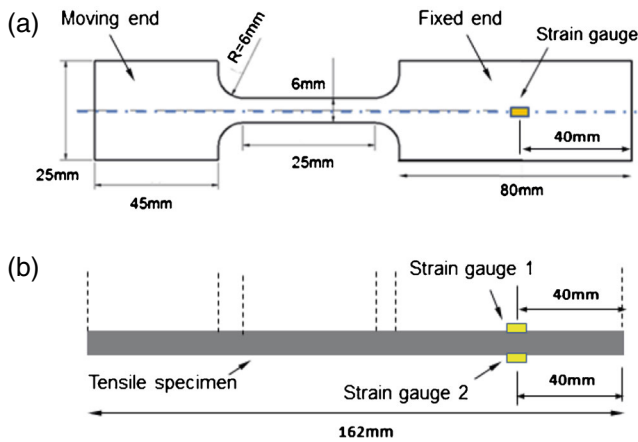


**Fig. 8** Optimized dimensions of a dynamic test specimen which eliminates ringing during dynamic tensile testing: **a** specimen dimensions, and **b** strain gauge locations

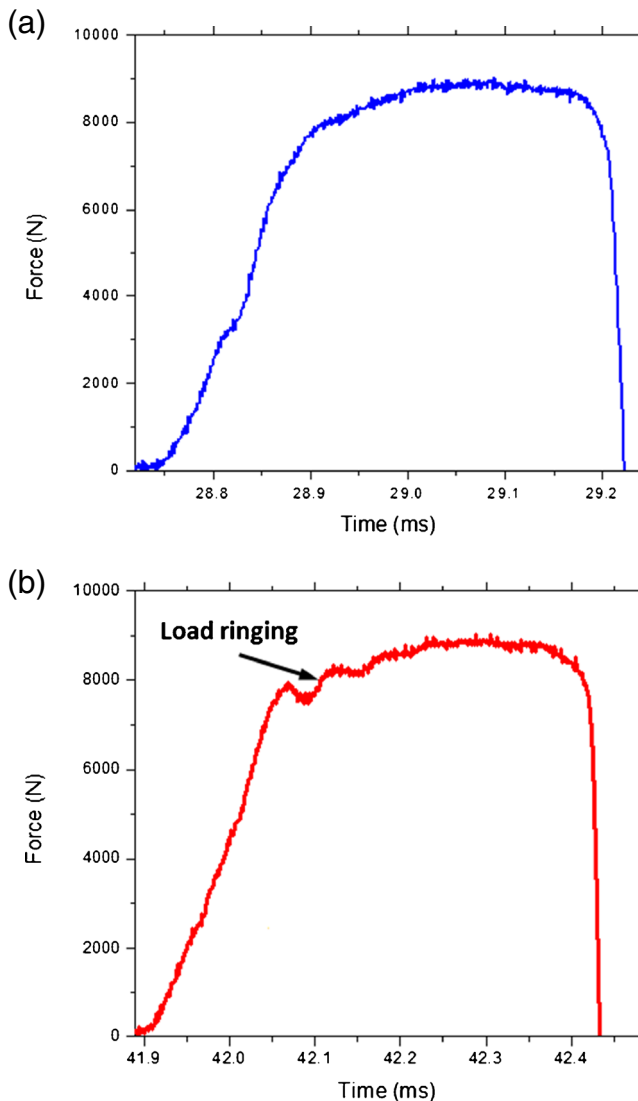


**Fig. 9** Force-time curves of test specimen (Q&P980) at  $\dot{\epsilon}$  of 500/s using gauge lengths ( $L$ ): **a** 25 mm, and **b** 35 mm

which was addressed in the above sections. The second is the stress state stability (or equilibrium) in the gauge section of the test specimen. To obtain valid stress–strain data in a material test, the specimen should be in a state of stress equilibrium, and undergo a homogeneous deformation in the gauge section. The condition of stress equilibrium in a specimen could be validated by a test with the strain gauges at both ends of the specimen (showing if the loads at both ends of the specimen are identical). However, in this section we propose a method to test the stress equilibrium of the specimen over the low dynamic range of strain rates based on analysis of the test duration.

Under quasi-static loading rates, the time for a stress wave to travel back and forth inside the specimen is small relative to the loading time and the specimen is therefore in a quasi-equilibrium state. In comparison, stress equilibrium may be difficult to achieve in a low dynamic test. Dynamic loading has to be introduced over a much shorter duration. The test duration in the low dynamic range could be comparable to the time needed for stress waves to travel round trip over the length of the load train. If the stresses build up in the specimen by relatively fewer stress waves, the condition of dynamic stress equilibrium may be violated.

The stress equilibrium in the Hopkinson bar test has been extensively studied [29–36]. It was observed that the loading rate, the specimen dimensions and the test material can affect the dynamic stress equilibrium. A slow loading rate, small specimen thickness or length, and high stress wave velocity (that travels inside the test material) were found to facilitate quicker stress equilibrium [37]. For example, polymer/plastic materials have a lower stress wave velocity relative to the steel material of interest in this study, and as such they need more time to reach dynamic stress equilibrium [38]. It has been established that in order to reach dynamic stress equilibrium, the stress wave should travel back and forth inside the test specimen more than three times [13]. The time needed for a specimen to achieve the dynamic stress equilibrium is given by

$$T = n \frac{2L}{c} \quad (12)$$

where  $L$  is the length of the specimen (distance between the movable grip and the fixed grip),  $c$  is the elastic stress wave speed of the material, and  $n$  is the number of round-trips of the stress wave ( $n \geq 3$  for reaching dynamic stress equilibrium). For the Q&P980 material having the recommended specimen dimensions (as shown in Fig. 8) by the combined experimental/theoretical approach presented in this study, the required time duration to achieve dynamic stress equilibrium is 0.107 ms per equation (12). As depicted in Fig. 11, using the recommended specimen dimensions, the time duration ( $T_e$ ) in the linear region (elastic stage) at 500/s is 0.13 ms. This meets the criterion for dynamic stress equilibrium.  $T_e$  increases for  $\dot{\epsilon} < 500/s$ .



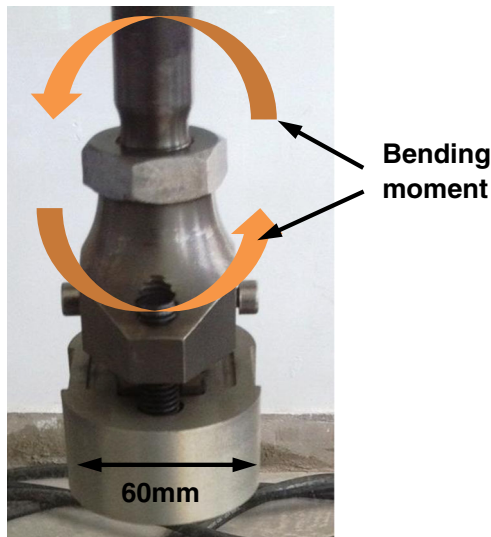


**Fig. 10** Upper fixture of the ZWICK HTM5020, connecting the upper (movable) end of the tensile specimen

Therefore, the Q&P980 tensile specimen with the recommended dimensions can reach the dynamic stress equilibrium at the elastic stage in a low dynamic test.

### Q&P980 Rate Sensitivity

Low dynamic tensile tests of the Q&P980 specimens were performed with the ZWICK dynamic tester using the optimized test specimen dimensions for minimizing ringing. According to the analysis in Section 3,  $\dot{\epsilon}_c = 120/s$ , i.e., the

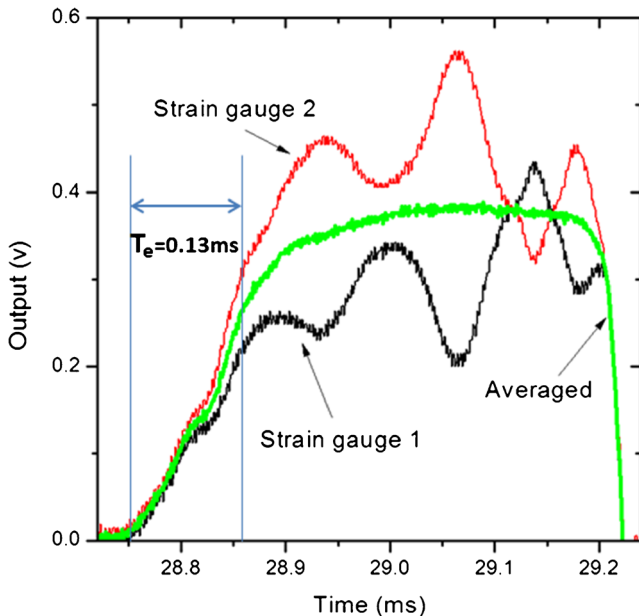


**Fig. 11** Strain gauge data at 500/s with the geometry shown in Fig. 8.  $T_e$  represents the time duration in the linear region (elastic stage). The green curve is the averaged data from the two strain gauge data sets, demonstrating the effect of bending on ringing artifact

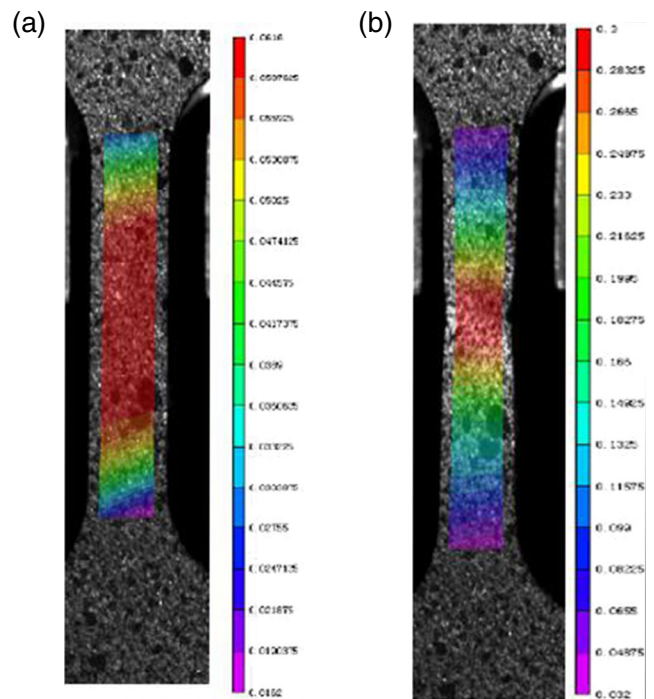


**Fig. 12** Contrast pattern for dynamic tensile tests, and typical DIC results (axial strain distribution contours) of Q&P980 at 500/s showing: **a** uniformity of the specimen deformation before necking, and **b** necking of the specimen. The contrast pattern applied to the tensile specimen surface consists of a thin layer of white spray paint and black dots, the diameters of which fall within the 0.1 mm to 0.5 mm range, randomly placed along the gauge length

ZWICK tester load cell can only be used for low dynamic tests at  $\dot{\epsilon} \leq 120/s$ . In this section, strain gauges were symmetrically attached on the two surfaces of each test specimen to measure the load in the fixed gripper end of the specimen for the whole low dynamic range ( $10/s \leq \dot{\epsilon} \leq 5 \times 10^2/s$ ). The load was extracted from the strain gauge using equation (8) and used to generate flow curves at the different strain rates. Note that  $\dot{\epsilon}$  was defined as the slope of the displacement-time curve recorded during testing, i.e., the velocity of the actuator (see Fig. 4), divided by the gauge length ( $L_I$ ) of the test specimen (see Fig. 6b). The specimen dimensions are shown in Fig. 8.

A single camera digital image correlation (DIC) method was utilized to measure the in-plane surface deformation and displacement fields of specimens deformed in the ZWICK load frame. This technique, as well as the stereo DIC technique, has been used to quantify deformation history and generate tensile flow curves [39, 40]. The input to the DIC algorithm requires a set of digital images that store the deformation history from one surface of the deforming tensile specimen, recorded at a fixed interval, up to fracture. Figure 12 shows the Q&P980 test specimen geometry and the surface from which digital images were taken with a high speed camera during testing. This surface was decorated prior to tensile testing with a black and white contrast pattern consisting of a thin layer of white spray paint and black dots with diameters in the 0.1 mm–0.5 mm

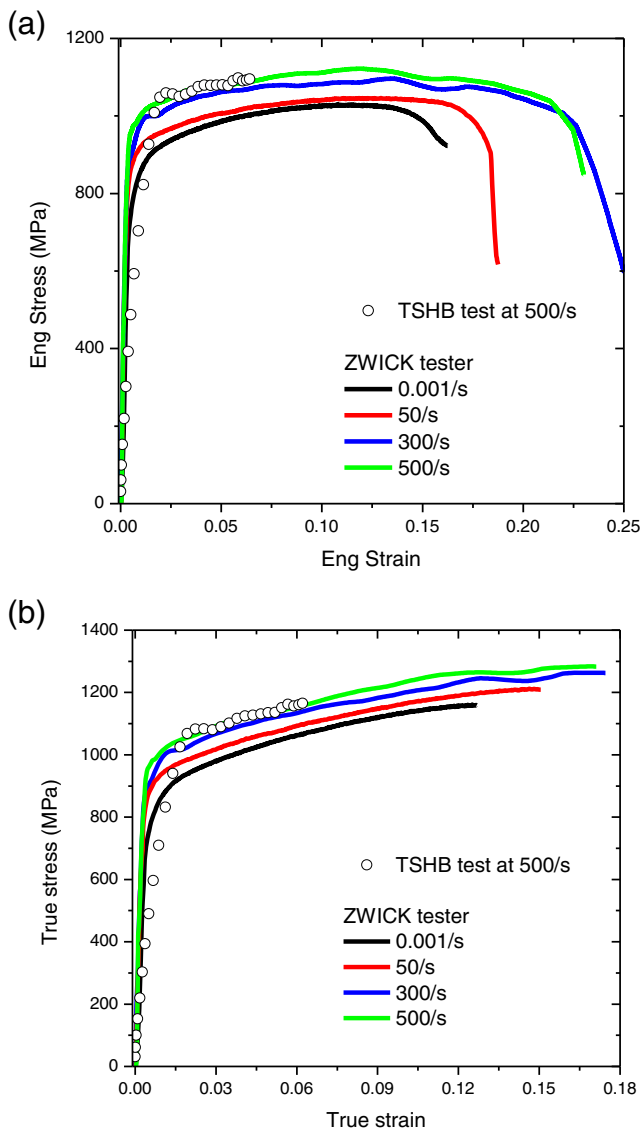


**Fig. 13** Summary of dynamic tensile tests results of Q&P980 specimens with the geometry shown in Fig. 8, compared to the TSHB test result at 500/s: **a** engineering strain – engineering stress, and **b** true strain – true stress

range. This contrast pattern facilitates DIC post-processing of the images in which displacement and strain fields are computed for the duration of the test.

Digital images were captured with a high-speed Phantom digital camera at a framing rate of 125,000 frames/second. The pixel density of each recorded .tif image was  $512 \times 256$  with a spatial resolution 0.015 mm/pixel. A trigger pulse from the displacement transducer on the ZWICK load frame was sent to the tester controller and the camera to synchronously record the force and displacement data for the tensile test specimen (i.e. each image was tagged with a load). The exposure time of the camera was 0.002 ms. At least 200 .tif images were captured for each low dynamic test. Post-processing was conducted with the DIC software VIC-2D

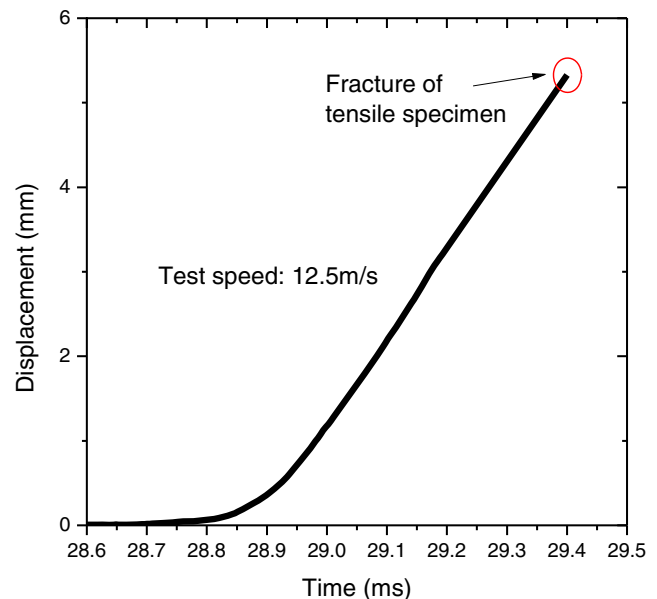
**Table 1** Dynamic test results of Q&P980 steel

Loading rate	0.2 % offset yield strength (MPa)	UTS (MPa)	Engineering fracture strain
$10^{-3}/s$	728.6 (5.8)	1047.6 (4.2)	0.199 (0.012)
0.1/s	741.5 (3.2)	1048.7 (2.1)	0.201 (0.009)
1/s	742.3 (2.8)	1050.0 (2.0)	0.196 (0.011)
10/s	745.2 (4.9)	1051.6 (3.3)	0.191 (0.015)
50/s	760.3 (6.9)	1056.2 (3.8)	0.189 (0.021)
100/s	769.9 (7.7)	1061.9 (5.9)	0.191 (0.011)
300/s	796.8 (10.2)	1067.8 (4.6)	0.208 (0.023)
500/s	805.5 (9.1)	1079.2 (9.3)	0.219 (0.031)

Average values (three specimens) are indicated, with standard deviations in parentheses

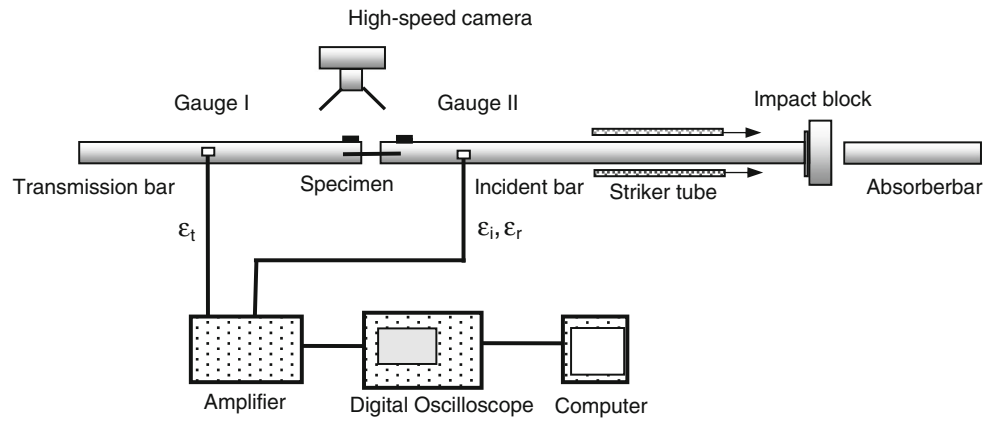
from Correlated Solutions [41]. Displacement and strain fields were computed from digital grids superimposed on each image in the DIC post-processing step, and then displayed as contour or strain maps. The pixel subset and grid point spacing were 15 and 5, respectively. The typical DIC results (axial strain distribution) of Q&P980 at 500/s, showing the uniformity of specimen deformation before necking and the necking of the specimen, were presented in Figs. 12a and b, respectively.

Figure 13 shows the low dynamic test results of Q&P980 by comparing the curves for  $\dot{\epsilon} = 0.001/s$ , 50/s, 300/s, and 500/s (averaged data from three repeats at each strain rate). Note that the input data for CAE modeling are generally required in



**Fig. 14** Displacement-time curve at the intermediate strain rates calculated by DIC

**Fig. 15** Schematic diagram of the tensile split Hopkinson bar (TSHB) used in this study



true strain – true stress format (as shown in Fig. 13b). Since significant stress localization occurs after necking, resulting in a non-uniaxial stress state, the data after necking would be invalid for CAE modeling. Table 1 compares the mechanical properties of Q&P980 steel at different  $\dot{\epsilon}$  values. It is clear from Fig. 13 and Table 1 that the Q&P980 shows an increase in yield strength with strain rate over the five orders-of-magnitude of  $\dot{\epsilon}$  that were examined in this study. Work-hardening appeared to be largely unaffected by  $\dot{\epsilon}$ . Figure 14 shows a representative displacement-time curve at  $\dot{\epsilon} = 500/s$ , computed in the DIC post-processing step. Note that we observed no apparent slippage between the specimen ends and the grips during the dynamic tests.

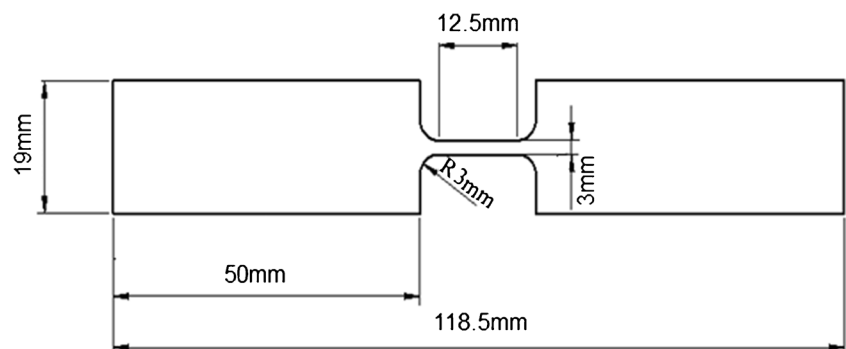
To evaluate the accuracy of the test data generated by following the combined theoretical/experimental approach to reducing ringing, we compare the data generated with the ZWICK load frame, with the results from a tensile split Hopkinson bar (TSHB) at  $\dot{\epsilon} = 500/s$ . The TSHB is considered to be a reliable device for generating the dynamic mechanical behavior of materials, and is often used for  $\dot{\epsilon} \geq 500/s$ . Unlike a servo-hydraulic test frame, however, ringing artifact is not an important issue for the TSHB test, since the TSHB equipment is designed to quickly achieve dynamic stress equilibrium with various techniques [42–44]. Figure 15 depicts the TSHB equipment, in which a hollow striker tube 300 mm in length is accelerated by compressed air and collides with the impact block producing a tensile pulse that propagates into the

incident bar, the tensile specimen and transmitted bar. The incident and transmitted bars of the TSHB equipment used in the present study are 2,750 mm and 1,500 mm in length, respectively. The incident, transmitted and reflected stress waves were measured with strain gauges. The signals from the strain gauges were monitored and acquired on an oscilloscope. The Q&P980 specimen geometry was dog-bone shaped as shown in Fig. 16. This was linked with the incident and transmitted bars in the TSHB by bolts, which are compact enough to prevent sliding of the specimen. Based on elastic stress wave theory [12, 13], the transmitted pulse was used to calculate the stress in the test specimen, but the reflected pulse was used to compute  $\dot{\epsilon}$  of the test specimen. The TSHB test results are presented in Fig. 13, compared to the test curves generated by ZWICK tester. The flow data were also extracted from Fig. 13a at elongations of 3 % and 7 %, and plotted in Fig. 17. The results from the two testing methods show very favorable agreement, which provides confidence in the validity of the developed testing technique at the low dynamic range detailed in this paper.

A power law relationship with the following form [45] is often used to describe the flow behavior for a metal alloy deformed within the low dynamic range:

$$\sigma = [K(\epsilon^p + \epsilon_0)^s] \left( \frac{\dot{\epsilon}^p}{\dot{\epsilon}_0} \right)^m \tag{13}$$

**Fig. 16** Specimen dimensions for the TSHB tests



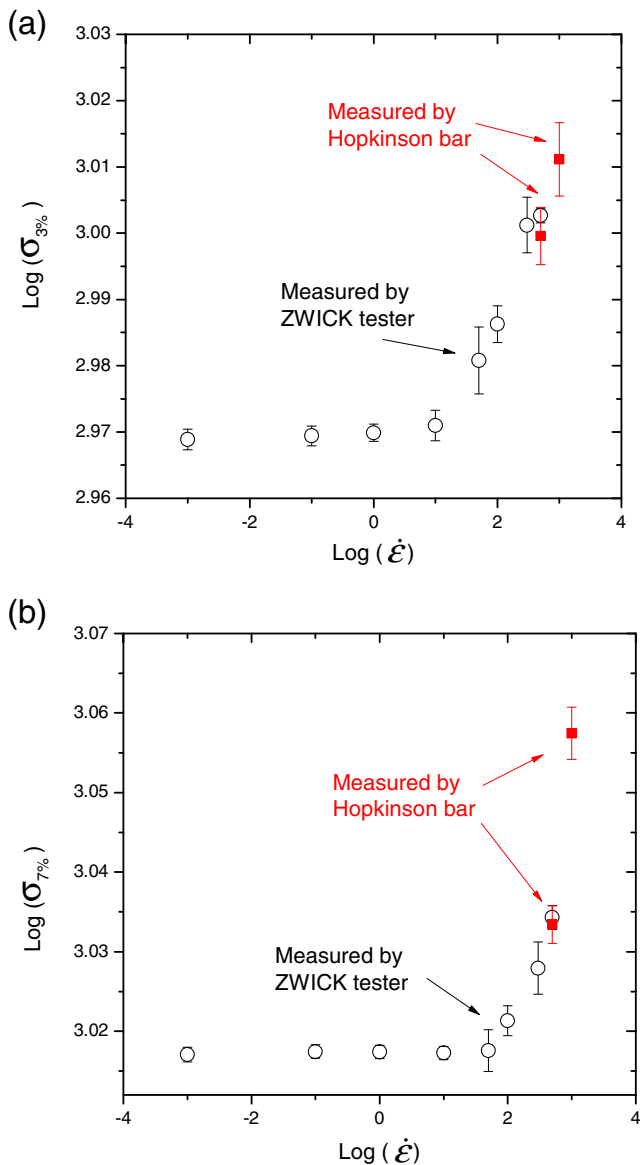


**Fig. 17** Strain rate sensitivity of Q&P980 at deformation levels of: **a** 3 %, and **b** 7 %.  $\sigma_{3\%}$  and  $\sigma_{7\%}$  represent the flow stresses at the deformation levels of 3 % and 7 %, respectively.  $\dot{\epsilon}$  is the nominal strain rate of the tensile test

where the material flow stress  $\sigma$  is a function of plastic strain rate  $\dot{\epsilon}^p$ , plastic strain  $\epsilon^p$ , material constants  $s$  and  $K$ , and strain rate sensitivity factor,  $m$ , the classical definition of which is

$$m = \frac{\ln(\sigma_1/\sigma_0)}{\ln(\dot{\epsilon}_1/\dot{\epsilon}_0)} \quad (14)$$

Here  $\sigma_1$  and  $\sigma_0$  represent the tensile flow stresses at two strain rates  $\dot{\epsilon}_1$  and  $\dot{\epsilon}_0$ , respectively. Figure 17 plots  $\ln \sigma$  vs.  $\ln \dot{\epsilon}$  curves.  $m$  was computed from the slope of the data curves in Fig. 17. It was determined that for the Q&P980 steel  $m = 2.17 \times 10^{-4}$  for  $\dot{\epsilon} \leq 10/s$ , and  $m = 0.0104$  for  $\dot{\epsilon} > 10/s$ . These

values are quite low compared to most steels which typically fall in the range of 0.02–0.2 [2]. A low  $m$  value has also been reported for the other TRIP steels [5].

Figure 17 exhibits a non-linear trend in  $m$ . It was found that  $m$  is shallow at  $\dot{\epsilon} \leq 10/s$ , and increases with increasing  $\dot{\epsilon}$ . The TSHPB data point at 1,000/s shows the continuation of the non-linear trend in  $m$  out of the low dynamic range (as plotted in Fig. 17). A similar behavior in  $m$  can also be found in Bruce et al. [19]. Boyce et al. [46] examined  $m$  for mild steel over a 195 K to 713 K temperature range. They suggested that for  $\dot{\epsilon} < 5,000/s$ , there were two regimes of  $m$ . At slower strain rates ( $\dot{\epsilon} \leq 10/s$ ) or higher temperatures (above 500 K), flow is controlled by long-range obstacles to dislocation motion and is largely strain rate insensitive. At lower temperatures (below 500 K) or higher strain rates ( $\dot{\epsilon} > 10/s$ ), weaker short range obstacles become controlling due to the time-dependent diffusion limited mechanisms such as climb which are necessary to overcome these short-range obstacles leading to a stronger strain rate dependence.

There are several constitutive flow models which consider strain rate sensitivity that have routinely been used to analyze dynamic tensile testing data. These include: the Johnson-Cook model [45], the Zerilli-Armstrong model [47], and the mechanical threshold stress model [48]. However, these models all assume a linear relation in  $m$ , and hence, the non-linear trend in  $m$  suggested in Fig. 17 and Table 1 cannot be predicted by the above constitutive equations. A more sophisticated flow model needs to be developed for low dynamic tensile testing with the servo-hydraulic dynamic load frame.

## Conclusions

In order to eliminate ringing of a load cell over the  $10/s \leq \dot{\epsilon} \leq 5 \times 10^2/s$  range in a servo-hydraulic tensile testing frame, the properties of the load train including the damping ratio ( $\zeta$ ) and the natural circular frequency ( $\omega_n$ ) which defines the load path from test specimen to load cell, were evaluated. It was recommended that  $\zeta$  falls in the  $0.6 \leq \zeta \leq 0.8$  range, or  $\omega_n \geq 4\omega$  (where  $\omega$  is the frequency of the load signal input to the load train) to eliminate ringing of the load cell. A combined theoretical/experimental approach based upon analysis of the servo-hydraulic tester load train was developed to optimize the specimen dimensions and minimize the ringing for tensile testing of thin sheet materials in the low dynamic range of strain rates ( $10/s \leq \dot{\epsilon} \leq 5 \times 10^2/s$ ). For the Q&P980 steel investigated in this study, a peak reduction in ringing of 90 % occurred at the high end of the low dynamic range (500/s) where ringing artifact is most severe over the low dynamic range. While the theoretical approach was developed with the ZWICK load frame (a servo-hydraulic tester), it can be readily

adapted to substantially reduce ringing in other servo-hydraulic load frames and with other sheet materials (in which the Young’s modulus is independent of strain rate). All that is required from the load frame is a testing speed over the low dynamic range and no slippage between the specimen ends and the grips during the test. The strain rate sensitivity factor ( $m$ ) was computed from the  $\ln \sigma$  vs.  $\ln \dot{\epsilon}$  curves of Q&P980 steel. For the Q&P980 steel,  $m = 2.17 \times 10^{-4}$  for  $\dot{\epsilon} \leq 10/s$ , and  $m = 0.0104$  for  $\dot{\epsilon} > 10/s$ .

**Acknowledgments** The authors would like to thank Dr. Yang Liu of Northeastern University, who prepared strain gauges for the dynamic tensile specimens, and provided hands-on assistance in operating the high-speed testing machine. Profs. Qing Zhou and Yong Xia of Tsinghua University, Drs. Kathy Wang and Li Sun of General Motors provided valuable comments and suggestions. Profs. Lei Wang and Yaping Zong of Northeastern University, and Prof. Dalian Chen of Ningbo University are acknowledged for their constant support of this project.

**Appendixes**

**Appendix 1: The Approach to Convert Frequency to Strain Rate**

Appendix Fig. 18 depicts a generic tensile test curve, in which  $\dot{\epsilon} = 10^{-3}/s$ . The circular frequency of the tensile test signal ( $\omega$ ) is calculated from [28],

$$\omega = \frac{\pi}{\Delta t} \tag{A-1}$$

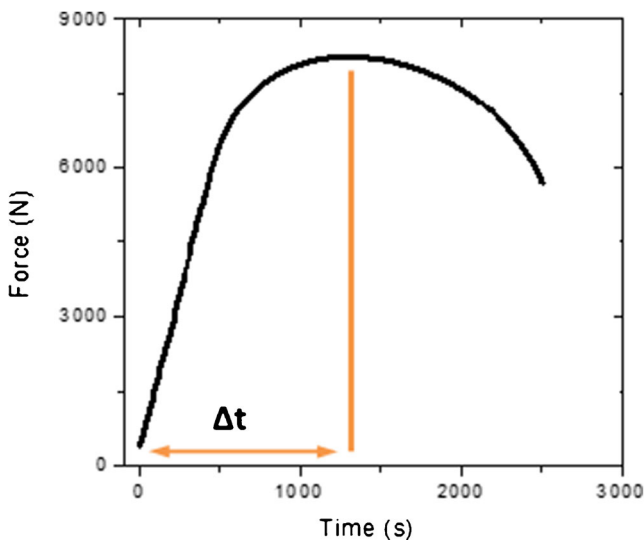


**Fig. 18** Input impulse signal in a typical tensile test of the steel material. Force is measured by the load cell in a static tensile test. Time is the tensile test duration recorded by the tensile tester.  $\Delta t$  represents the load rise time (from the start of the test to the end of uniform elongation) of the force-time response of the test specimen

where  $\Delta t$  represents the load rise time (from the start of the test to the end of uniform elongation) of the force-time response of the test specimen. It was assumed that there is no change in uniform elongation over the range of strain rates of interest in this paper ( $10^{-5}/s \leq \dot{\epsilon} \leq 5 \times 10^2/s$ ) and  $\dot{\epsilon}$  stays constant during a tensile test. Therefore,

$$\dot{\epsilon}_q \Delta t_q = \dot{\epsilon}_d \Delta t_d \tag{A-2}$$

where  $\dot{\epsilon}_q$  and  $\dot{\epsilon}_d$  are a quasi-static strain rate and a low dynamic strain rate, respectively;  $\Delta t_q$  and  $\Delta t_d$  are the load rise times corresponding to  $\dot{\epsilon}_q$  and  $\dot{\epsilon}_d$ , respectively. Furthermore,

$$\frac{\Delta t_q}{\Delta t_d} = \frac{\omega_d}{\omega_q} \tag{A-3}$$

where  $\omega_q$  and  $\omega_d$  represent the circular frequencies at a quasi-static strain rate and at a low dynamic strain rate, respectively. Therefore,  $\dot{\epsilon}_d$  can be calculated as

$$\dot{\epsilon}_d = \dot{\epsilon}_q \frac{\omega_d}{\omega_q} \tag{A-4}$$

In order to convert  $\omega_d$  to  $\dot{\epsilon}_d$ , first  $\omega_q$  and  $\dot{\epsilon}_q$  need to be determined from a conventional quasi-static tensile test. As an example, a quasi-static tensile test of the Q&P980 was performed according to the ASTM E8 standard [49]. It was determined that,  $\Delta t_q = 151$  s and  $\omega_q = 2.07 \times 10^{-2}$  Hz, at  $\dot{\epsilon}_q = 10^{-3}/s$ . Solving equation (A-4),  $\dot{\epsilon}_d$  is equal to 120/s, corresponding to  $\omega_d$  of 2.48 kHz.

**Appendix 2: Material**

A third generation AHSS was considered in the study, viz. Q&P980 manufactured by Shanghai Baosteel Group Corporation. The Q&P process was developed by the Colorado School of Mines [50–52] as a means for producing a third generation advanced high strength steel with superior combinations of strength and ductility. The Q&P980 microstructure consists of ferrite, martensite, and carbon-enriched retained austenite [53]. The chemical composition of Q&P steel is listed in Appendix Table 2 [54].

**Table 2** Chemical composition (wt%) of Q&P980 steel [52]

C	Si	Mn	P	S	Al	N
0.20	1.49	1.82	0.017	0.0043	0.046	0.0039



## References

1. Davis JR (ed). Tensile Testing. Second Edition, ASM International, Materials Park, OH, 44073-0002
2. Hertzberg RW (1989) Deformation and fracture mechanics of engineering materials, 3rd edn. John Wiley & Sons, New York
3. Meyers M (1994) Dynamic behavior of materials. John Wiley&Sons, New York, p P. 299
4. Huh H, Lim JH, Park SH (2009) High speed tensile test of steel sheets for the stress-strain curve at the intermediate strain rate. *Int J Automot Technol* 10:195–204
5. Larour P (2010) Strain rate sensitivity of automotive sheet steels: influence of plastic strain rate, temperature, microstructure, bake hardening and pre-strain. Ph.D. Thesis, Aachen University
6. Boyce BL, Crenshaw TB, Dilmore MF (2007) The Strain-rate sensitivity of high-strength high-toughness steels. Sandia Report SAND2007-0036, Sandia National Laboratories Albuquerque, New Mexico 87185
7. Shi MF, Meuleman DJ (1992) Strain rate sensitivity of automotive steels. Society of Automotive Engineers 920245, Warrendale
8. Bardelcik A, Worswick MJ, Winkler S, Wells MA (2012) A strain rate sensitive constitutive model for quenched boron steel with tailored properties. *Int J Impact Eng* 50:49–62
9. Huh H, Kim SB, Song JH, Lim JH (2008) Dynamic tensile characteristics of TRIP-type and DP-type steel sheets for an auto-body. *Int J Mech Sci* 50:918–931
10. Zhu D, Mobasher B, Rajan SD, Peralta P (2011) Characterization of dynamic tensile testing using aluminum alloy 6061-T6 at intermediate strain rates. *ASCE J Eng Mech* 137:669–679
11. Picua RC, Vinczeb G, Ozturka F, Graciob JJ, Barlatb F, Maniatty AM (2005) Strain rate sensitivity of commercial aluminum alloy AA5182-O. *Mat Sci Eng A* 390:334–343
12. Chen W, Song B (2011) Split Hopkinson (Kolsky) Bar. Design, testing and applications. Springer, New York
13. Gray GT III (2000) Classic split Hopkinson pressure bar testing. Mechanical testing and evaluation handbook, vol.8. American Society for Metals, Materials Park, pp 488–496
14. Xiao X (2008) Dynamic tensile testing of plastic materials. *Polym Test* 27:164–178
15. Recommendations for dynamic tensile testing of sheet steels (2008) IISI High Strain Rate Experts Group
16. High strain rate tensile testing of polymers (2008) Society of Automotive Engineers SAE Standard J2749. USA
17. Maier M (2003) Recent improvements in experimental investigation and parameter fitting for cellular materials subjected to crash loads. *Compos Sci Tech* 63:2007–2012
18. Yan B (2006) Recommended practice for dynamic testing for sheet steels development and round robin tests. Society of Automotive Engineers 2006-01-0120, Warrendale
19. Bruce DM, Matlock DK, Speer JG, De AK (2004) Assessment of the strain-rate-dependent tensile properties of automotive sheet steels. Society of Automotive Engineers 2004-01-0507, Warrendale
20. Fitoussi J (2005) Experimental methodology for high strain-rates tensile behavior analysis of polymer matrix composites. *Compos Sci Tech* 65:2174–2188
21. Song B, Chen W, Lu WY (2007) Compressive mechanical response of a low-density epoxy foam at various strain rates. *J Mat Sci* 42: 7502–7507
22. Xiao X (2008) Analysis of dynamic tensile testing. Proc. of the XIth International Congress and Exposition, Orlando, Florida USA, Society for Experimental Mechanics Inc. Bethel, CT 06801-1405
23. Zhu D, Rajan SD, Mobasher B, Peled A, Mignolet M (2011) Modal analysis of a servo hydraulic high speed machine and its application to dynamic tensile testing at an intermediate strain rate. *Exp Mech* 51: 1347–1363
24. Bleck W, Schael I (2000) Determination of crash-relevant material parameters by dynamic tensile tests. *Steel Research* 71:173–178
25. Wong C (2005) IISI-AutoCo Round-Robin Dynamic Tensile Testing Project. International Iron and Steel Institute Report
26. Irvine T. Damping properties of materials. <http://www.cs.wright.edu/~jlater/SDTCOutreachWebsite/damping%20properties%20of%20materials.pdf>.
27. Sun X, Khaleel MA (2007) Dynamic strength evaluations for self-piercing rivets and resistance spot welds joining similar and dissimilar metals. *Int J Impact Eng* 34:1668–1682
28. Wang K (2010) Research on testing techniques for materials and structures. Tsinghua University, Beijing
29. Chen W, Song B, Frew DJ, Forrestal MJ (2003) Dynamic small strain measurements of a metal specimen with a split Hopkinson pressure bar. *Exp Mech* 43:20–23
30. Casem D, Weerasooriya T, Moy P (2005) Inertial effects of quartz force transducers embedded in a split Hopkinson pressure bar. *Exp Mech* 45:368–376
31. Wang ZG, Meyer LW (2010) On the plastic wave propagation along the specimen length in SHPB test. *Exp Mech* 50:1061–1074
32. Warren TL, Forrestal MJ (2010) Comments on the effect of radial inertia in the Kolsky bar test for an incompressible material. *Exp Mech* 50:1253–1255
33. Luo H, Lu H, Cooper WL, Komanduri R (2011) Effect of mass density on the compressive behavior of dry sand under confinement at high strain rates. *Exp Mech* 51:1499–1510
34. Casem DT, Grunschel SE, Schuster BE (2012) Normal and transverse displacement interferometers applied to small diameter Kolsky bars. *Exp Mech* 52:173–184
35. Wang E, On T, Lambros J (2013) An experimental study of the dynamic elasto-plastic contact behavior of dimer metallic granules. *Exp Mech* 53:883–892
36. Gary G, Mohr D (2013) Modified Kolsky formulas for an increased measurement duration of SHPB systems. *Exp Mech* 53:713–717
37. Song B, Chen W (2004) Dynamic stress equilibration in split Hopkinson pressure bar tests on soft materials. *Exp Mech* 44:300–312
38. Brown EN, Willms RB, Gray GT III, Rae PJ, Cady CM, Vecchio KS, Flowers J, Martinez MY (2007) Influence of molecular conformation on the constitutive response of polyethylene: a comparison of HDPE, UHMWPE, and PEX. *Exp Mech* 47:381–393
39. Coryell J, Savic V, Hector L, Mishra S (2013) Temperature effects on the deformation and fracture of a Quenched-and-Partitioned steel. Society of Automotive Engineers 2013-01-0610, Warrendale
40. Hector L, Savic V (2013) Tensile material properties of fabrics for vehicle interiors from digital image correlation. Society of Automotive Engineers 2013-01-1422, Warrendale
41. Vic-2D User Guide (2009). [http://correlatedsolutions.com/support/index.php?\\_m=downloads&\\_a=viewdownload&downloaditemid=2&nav=0](http://correlatedsolutions.com/support/index.php?_m=downloads&_a=viewdownload&downloaditemid=2&nav=0)
42. Chen W, Lu F, Cheng M (2002) Tension and compression tests of two polymers under quasi-static and dynamic loading. *Polym Test* 21: 113–121
43. Chen W, Zhang B, Forestal MJ (1999) A split Hopkinson pressure bar technique for low-impedance materials. *Exp Mech* 39:81–88
44. Zhao H, Gary G, Klepaczko JR (1997) On the use of a viscoelastic split Hopkinson pressure bar. *Int J Impact Eng* 19:319–330
45. Johnson GR, Cook WH (1983) A constitutive model and data for metals subjected to large strains, high strain rates, and high temperatures. In: Proceedings of the seventh international symposium on ballistics. The Netherlands: Am Def Prep Org (ADPA) 541–547
46. Boyce BL, Dilmore MF (2009) The dynamic tensile behavior of tough, ultrahigh-strength steels at strain-rates from 0.0002/s to 200/s. *Int J Impact Eng* 36:263–271

47. Zerilli FJ, Armstrong RW (1987) Dislocation-mechanics-based constitutive relations for materials dynamics calculations. *J Appl Phys* 61:1816–1825
48. Follansbee PS, Kocks UF (1988) Constitutive description of the deformation of copper based on the use of the mechanical threshold stress as an internal state variable. *Acta Met* 36:81–93
49. ASTM E8/E8M–09 (2009) Standard test methods for tension testing of metallic materials. ASTM International, West Conshohocken
50. Speer JG, Matlock DK, De Cooman BC, Schroth JG (2003) Carbon partitioning into austenite after martensite transformation. *Acta Mater* 51:2611–2622
51. Clark AJ, Speer JG, Miller MK, Hackenberg RE, Edmonds DV, Matlock DK, Rizzo FC, Clarke KD (2008) Carbon partitioning to austenite from martensite or bainite during the quench and partition (Q&P) process: a critical assessment. *Acta Mater* 56:16–22
52. Speer JG, Rizzo-Assunção FC, Matlock DK, Edmonds DV (2005) The “quenching and partitioning” process: background and recent progress. *Mater Res* 8:417–423
53. Edmonds DV, Miller HK, Rizzo FC, Clarke AJ, Matlock DK, Speer JG (2007) Microstructural features of quenching and partitioning: a new martensitic steel heat treatment. *Mater Sci Forum* 5:4819–4825
54. Coryell J, Campbell J, Savic V, Bradley J, Mishra S, Tiwari S, Hector L (2012) Tensile deformation of quenched and partitioned steel – a third generation high strength steel. *Minerals Met Mater Soc* 2:555–562